Spatial averaging for small molecule diffusion in condensed phase environments

Nuria Plattner, J. D. Doll, and Markus Meuwly

Citation: The Journal of Chemical Physics **133**, 044506 (2010); doi: 10.1063/1.3458639
View online: http://dx.doi.org/10.1063/1.3458639
View Table of Contents: http://scitation.aip.org/content/aip/journal/jcp/133/4?ver=pdfcov
Published by the AIP Publishing

Spatial averaging for small molecule diffusion in condensed phase environments

Nuria Plattner,[1] J. D. Doll,[2] and Markus Meuwly[1,2,a)]
[1]*Department of Chemistry, University of Basel, Klingelbergstrasse 80, CH-4056 Basel, Switzerland*
[2]*Department of Chemistry, Brown University, Providence, Rhode Island 02912, USA*

(Received 16 March 2010; accepted 9 June 2010; published online 26 July 2010)

Spatial averaging is a new approach for sampling rare-event problems. The approach modifies the importance function which improves the sampling efficiency while keeping a defined relation to the original statistical distribution. In this work, spatial averaging is applied to multidimensional systems for typical problems arising in physical chemistry. They include (I) a CO molecule diffusing on an amorphous ice surface, (II) a hydrogen molecule probing favorable positions in amorphous ice, and (III) CO migration in myoglobin. The systems encompass a wide range of energy barriers and for all of them spatial averaging is found to outperform conventional Metropolis Monte Carlo. It is also found that optimal simulation parameters are surprisingly similar for the different systems studied, in particular, the radius of the point cloud over which the potential energy function is averaged. For H_2 diffusing in amorphous ice it is found that facile migration is possible which is in agreement with previous suggestions from experiment. The free energy barriers involved are typically lower than 1 kcal/mol. Spatial averaging simulations for CO in myoglobin are able to locate all currently characterized metastable states. Overall, it is found that spatial averaging considerably improves the sampling of configurational space. © *2010 American Institute of Physics*. [doi:10.1063/1.3458639]

I. INTRODUCTION

Characterizing the diffusion of small probe molecules in heterogeneous environments or on surfaces is important for understanding adsorption, desorption, surface chemical reactions, or migration pathways. Such processes usually take place between different sites/defects (on surfaces) or different pockets (in proteins), which are separated by barriers, typically of height $>k_BT$, where k_B is the Boltzmann constant and T is the temperature. Under such circumstances the transition between neighboring sites is an activated process and may be a rare event.

Rare events typically occur on short time scales but with very low probability. Thus, investigating such processes is a challenge because the waiting time between two events τ_w is typically considerably longer than the characteristic time scales τ_j on which motion in the system occurs. One example is the diffusion of small probe molecules in disordered environments. The typical time scale of molecular vibration and rotation is on the order of femtoseconds, whereas transit times between two metastable states in the system can be nanoseconds or longer. Other well-known examples are activated processes (chemical reactions) in the condensed phase where the motions of the particles take place on the femto- and picosecond time scales, but rate constants are on the seconds time scale. In molecular simulations the fact that an event is rare crucially depends on our ability to sample a process sufficiently often (Monte Carlo) or over sufficiently long time (molecular dynamics). As such, the classification of events into "frequent" or "rare" can also be viewed as our ability to find appropriate sampling schemes which increase the probability of a particular event to occur. Examples for such "enhanced" sampling methods include metadynamics,[1] umbrella sampling,[2] transition path sampling,[3] or multicanonical sampling.[4]

Typical examples of rare events are (I) the diffusion of CO on amorphous ice surfaces, (II) the diffusion of H_2 in amorphous ice, and (III) the diffusion of CO in myoglobin (Mb). Each of these problems is characterized by typical spatial length scales and barriers between the metastable states. In the present work we apply spatial averaging[5] to examples (I)–(III), each of which poses specific problems in sampling configuration space. Spatial averaging has been recently presented as a Monte Carlo (MC) implementation or to be used together with molecular dynamics simulations. Inherent to the method is a length scale which determines the maximal range over which sampling is enhanced. Thus, some knowledge about the topology of phase space of the particular problem at hand is of advantage, but no detailed information about the system and its reaction coordinates are required. The physical relevance of each of the systems is briefly summarized in the following.

(I) The interaction between CO and amorphous ice is important in astronomy contexts where sticking coefficients are of primary interest for reactions that take place on amorphous ice surfaces.[6] The energetic barriers between neighboring positions in this system are low since the energy difference between different positions on the surface originate only from Van-der-Waals (VdW) interactions and electrostatics, and the VdW interactions are very similar for neighboring po-

a)Electronic mail: m.meuwly@unibas.ch.

sitions on the surface. The desorption energy in contrast is significantly higher.

(II) Ultraviolet radiation promotes the formation of H_2 in amorphous ice and converts crystalline ice to the amorphous form.[7] Micropores may be rather important in this process since there is an increased probability of an encounter between two H-atoms within the pores[8] and the dissociation probability of surface water molecules is higher than those in the bulk. Thus, the H_2 production probability may be enhanced within the pores. In addition, unimolecular decay channels can produce hydrogen molecules directly at pore surfaces. Contrary to CO on amorphous ice the energetic barriers are higher in this system and steep since they are dominated by the repulsive part of the Lennard-Jones potential.

(III) The diffusion of diatomic ligands such as oxygen, CO, and NO in myoglobin has been extensively studied by experiment and theory in the past.[9–13] Finding all possible pathways and favorable pockets for a diatomic molecule in a protein is a challenging sampling problem which can be divided into two parts: (A) finding all possible myoglobin conformations and (B) for a given conformation finding all favorable positions and pathways for the ligand. This formal separation is not necessary because the dynamics of the protein and that of the diffusing ligand might be coupled in certain regions of phase space. In other words, the protein dynamics differs when an unbound ligand is present or absent. This has been previously found for NO migration in truncated hemoglobin where extensive sampling has found all experimentally and computationally known ligand binding sites,[14] whereas alternative and less rigorous sampling schemes only found particular subsets.[12,15] The energy landscape can be expected to be more complex than for H_2 in amorphous ice, given the importance of conformational sampling, in particular at temperatures beyond the glass transition.

The specific questions asked in the following are: What part of phase space is sampled by conventional sampling and spatial averaging? How efficiently is this space sampled? For CO adsorbed on an amorphous ice surface, spatial averaging should provide a broader distribution of sampled positions parallel and perpendicular to the surface. Problems (II) and (III) both consist of finding cavities accessible to a small molecule. However, the height of the barriers is quite different in the two cases. The efficiency of spatial averaging compared to conventional MC is quantified by monitoring the rate of diffusion as a function of the number of MC steps (see Sec. II D). This quantity allows us to evaluate the average number of moves required to sample a given distance from the initial position and therefore provides an unambiguous efficiency comparison of standard MC and spatial averaging. Another issue to consider in terms of efficiency is the computational overhead required for spatial averaging in each MC step compared to conventional MC. This depends sensitively on details of how the computations are carried out, in particular for spatial averaging. Therefore an unambiguous comparison is difficult. Additional details are provided in Sec. II D.

This work is structured as follows. First, the computational realizations of all systems investigated are presented and details of the implementation of spatial averaging are provided. Next, results for the three systems are presented and discussed. Finally, they are discussed in a wider context and conclusions are drawn.

II. COMPUTATIONAL METHODS

In the following the computational models for the three systems and the interaction potentials are first presented. Next, the spatial averaging strategy and its implementation are discussed. All simulations presented and discussed were carried out with the CHARMM program[16] with suitable extensions to allow the sampling strategies described below.

A. The model systems studied

1. CO on amorphous ice

For CO on an amorphous ice surface a hexagonal ice cube with 1024 water molecules and dimensions of $35\times31\times29$ Å^3 was heated to 300 K and equilibrated during 50 ps in the *NPT* ensemble. Simulation time and temperature are sufficient to break the symmetry of the ice structure. The system was then cooled to 100 K and equilibrated during additional 50 ps. To create a surface, the periodic boundaries were set to the dimensions of the ice cube of 33 and 30 Å in two dimensions. To the third dimension (28 Å), an additional 20 Å was added. This system was equilibrated for 100 ps at 20 K in the *NVT* ensemble. A CO molecule was then inserted in the center of the ice cube surface and the structure was optimized. For the *NPT* simulations in this and other sections, a Nose–Hoover thermostat[17,18] was used. For all *NVT* simulations, the weak coupling method of Berendsen[19] was applied.

2. H_2 in amorphous ice

For H_2 in amorphous ice the structure at the end of the 100 K equilibration run (see above) was used. The dimensions of the box were adjusted in the same way as described above and equilibrated in the *NVT* ensemble during 200 ps at 300 K and during 100 ps at 100 K. This leads to an extension of the ice in one dimension and creates cavities in the ice structure. Finally, a hydrogen molecule was inserted in the center of the cube and the structure was optimized.

3. CO in myoglobin

Simulations for CO in myoglobin were started from the x-ray structure (Protein Data Bank reference 1MBC)[20] to which hydrogen atoms were added. First, the positions of the hydrogen atoms were optimized with heavy atoms frozen at their crystallographic positions. Next, the protein was solvated in a previously equilibrated waterbox with dimensions of $57\times51\times39$ Å^3, which was heated to 300 K and equilibrated during 100 ps in the *NPT* ensemble. A cutoff of 12 Å was used for the nonbonded interactions.

TABLE I. Distributed multipole parameters for H_2. The values refer to the equilibrium position given by the coordinates.

	Coordinate (Å)	Dipole (ea_0)	Quadrupole (ea_0^2)	Octopole (ea_0^3)
H1	0.371 478	−0.069 097	0.318 182	−0.031 723
H2	−0.371 478	0.069 097	0.318 182	0.031 723

B. Force field parameters and potentials

For the ice systems, the TIP3P water model[21] was used together with the SHAKE algorithm[22] for constraining the O–H bonds to allow a timestep of 1 fs. For CO and H_2, atomic multipole moments up to octopole were used. The parameters for H_2 given in Table I have been obtained from B3LYP aug-cc-pVTZ calculations with the GAUSSIAN (Ref. 23) program and using GDMA (Ref. 24) to extract the multipole moments. Those for CO are described elsewhere.[25] For the simulations with atomic multipole moments, the corresponding interaction terms have been implemented in the CHARMM program[16] based on the published terms.[26] For CO in myoglobin, the standard CHARMM parameters were used for the amino acids, the heme unit, and the ligand.[27,28]

C. Spatial averaging and its implementation

Stochastic quadrature methods typically utilize random walk procedures to perform a statistical sampling of a specified probability density. When the "important" regions of the integration volume are well-connected, random walk procedures such as the Metropolis technique are adequate. In problems where one is faced with distributions that have multiple, isolated regions of importance, however, the performance of such methods can become problematic and special care must be exercised to deal with the "sparse" or "rare-event" sampling issues that are involved.

As discussed elsewhere[5] it is possible to construct a family of densities related to the original distribution with two important properties:

- the integrals of these modified densities over all space are identical to those of the original distribution, and
- the spatial averaging is designed in a manner that the resulting, modified densities are more "connected" and hence can be more easily sampled than the original density.

In the spatial averaging approach the overall strategy is thus to modify the underlying probability density itself rather than to create a computational ensemble that spans a range of control parameters, a strategy utilized in parallel tempering techniques.[29]

If the density to be sampled is $\rho(x)$, a family of modified densities having the required properties can be obtained by writing (using a pseudo-one-dimensional notation)

$$\rho(x,\varepsilon) = \int P_\varepsilon(y)\rho(x+y)dy, \tag{1}$$

where $P_\varepsilon(y)$ is a (normalized) probability distribution with a length scale ε. Although we will typically take it to be Gaussian in nature, aside from the requirement that it can be normalized the choice of this distribution is essentially arbitrary. Integrating Eq. (1) over all space it is easy to show that the integrals of the original and modified densities, $\rho(x,0)$ and $\rho(x,\varepsilon)$, respectively, are equal for all values of ε provided only that

- it is permissible to invert the orders of integration for x and y, and
- that the integration domain is infinite (or that the density is periodic over the interval in question).

The family of densities defined by Eq. (1) thus represents a set of norm-conserving densities whose thermodynamic properties are closely linked to those of the original distribution. Moreover, because the averaging process tends to move density from high to low probability regions, the modified densities tend to be "more connected" than the original one and hence more easily sampled.

Spatial averaging was implemented into the CHARMM MC module[30] and is based on the penalty Monte Carlo method[31] which allows us to combine the Metropolis algorithm with Monte Carlo integration steps. To modify the MC importance function, a variable number of configurations N_ε is generated for each coordinate of the atoms for which the MC sampling is carried out. The distribution of the configurations is Gaussian $\propto \exp^{-(x-x_0)^2/2W_\varepsilon^2}$, centered around the initial coordinate x_0 and with width W_ε. Each MC move is then applied to all N_ε configurations. The move is accepted for the entire distribution if the average energy difference between all pairs of configurations satisfies the Metropolis criterion[32] and if the variance in energy difference remains small. In detail, spatial averaging includes the following steps.

(1) Generate a trial configuration based on the given configuration and for the given type of MC move (this step is identical to conventional MC).
(2) Around the initial configuration $\vec{x}_0$, generate a Gaussian distribution of N_ε points for M_ε sets of points with standard deviation W_ε in configuration space. The Gaussian random numbers are generated using the random number generator available in the CHARMM program. They are transformed into Gaussian distributed random numbers of zero mean and standard deviation W_ε according to the algorithm of Box and Muller.[33] The Gaussian distributed random numbers $\rho(\vec{x}_i)$ are then added to the coordinates $\vec{x}_0$ in each direction. The procedure is repeated $N_\varepsilon * M_\varepsilon$ times to generate all points of the spatial averaging distribution.
(3) Carry out the MC move for all N_ε points in all M_ε sets and calculate for each point the old energy $E_{\text{old}}^{(n,m)}$ and the new energy $E_{\text{new}}^{(n,m)}$ with corresponding Boltzmann weights $E_{\text{old,exp}}^{(n,m)} = e^{-\beta * E_{\text{old}}^{(n,m)}}$ and $E_{\text{new,exp}}^{(n,m)} = e^{-\beta * E_{\text{new}}^{(n,m)}}$.

(4) For each of the M_ε sets, calculate $S^m_{\text{old}}=\Sigma^{N_\varepsilon}_{n=0}E^{(n,m)}_{\text{old,exp}}$ and $S^m_{\text{new}}=\Sigma^{N_\varepsilon}_{n=0}E^{(n,m)}_{\text{new,exp}}$.
(5) For each of the M_ε sets, calculate $\delta_m=-\ln(S^m_{\text{new}}/S^m_{\text{old}})$.
(6) Calculate

$$\delta = 1/M_\varepsilon \Sigma_m \delta_m \quad \text{and}$$

$$\sigma^2 = (1/[M_\varepsilon * (M_\varepsilon - 1)])\Sigma^N_i(\delta_m - \delta)^2.$$

(7) For acceptance or rejection, ΔE in the Metropolis algorithm is replaced by $\delta+(\sigma^2/2)$.

A spatial averaging MC simulation is therefore characterized by specific values for W_ε, M_ε, and N_ε. In the following, a particular simulation will be described as a tupel $[W_\varepsilon, M_\varepsilon, N_\varepsilon]$. With this nomenclature, conventional MC formally corresponds to [0.0,1,1], where $W_\varepsilon=0.0$ in the Gaussian distribution has to be understood as a δ-function and $M_\varepsilon=1$ is not required in step (6) of the above scheme, i.e., only $N_\varepsilon=1$ has an actual meaning. As in all MC simulations a maximal range $x_t^{\max}$ for a move for a particular coordinate is chosen. In the present implementation, spatial averaging includes only the degrees of freedom selected for the MC moves. It has to be noted that in general, spatial averaging could also include other system coordinates.

D. Analysis of MC efficiency

The MC efficiency is evaluated using the MC diffusion $\sigma(s)$,

$$\sigma(s) = \frac{1}{N_{\max}} \sum_{i=1}^{N_{\max}} |\vec{r}_i - \vec{r}_{i+s}|^2, \tag{2}$$

with $s=0,\ldots,s_{\max}$, where s is the number of MC moves between two steps, $\vec{r}$ is the coordinate vector for the molecule of interest, and $N_{\max}$ is the number of evaluation steps, which can maximally be half of the number of MC frames. $\sigma(s)$ is the MC-equivalent of diffusion whereas $\sigma_{\text{rms}}(s)=\sqrt{\sigma(s)}$ reports directly on the distance traveled by the molecule.

For periodic systems with nonbonded cutoffs—which are the approach chosen for the systems studied here—the computing time required in each MC step is determined mainly by two factors: (1) the generation of nonbonded and image atom lists and (2) the energy evaluation based on these lists. The computational effort required to generate the lists is equal for standard MC and spatial averaging. The number of energy evaluations is proportional to $N_\varepsilon * M_\varepsilon$. Therefore the relative computational overhead used for spatial averaging for a given system depends on the ratio of the time needed to generate nonbonded lists versus the time of a single energy evaluation. It is difficult to evaluate this quantity in an unambiguous way since it depends on the list update frequency and the $N_\varepsilon * M_\varepsilon$ sampling points.

III. RESULTS

In the following, sampling of the available configurational space for three different systems is characterized and explored, and the physical insight for systems (I)–(III) gained by the simulations is discussed. Conventional and spatial averaging results are compared, and advantages and disadvantages of either approach are discussed. It will be shown that previous knowledge about the properties and topologies of the systems is advantageous in choosing suitable simulation conditions, but no detailed information about the system is required.

A. CO on amorphous ice surface

Previously, the sampling of CO in amorphous ice was characterized based on molecular dynamics (MD) simulations.[34] By comparing with experimental results from infrared spectroscopy[35,36] it was found that CO molecules can be largely classified into occupying interstitial or substitutional sites, respectively. This leads to two bands in the infrared spectrum of CO. However, for increasing CO concentration additional effects, such as the mutual influence of the CO molecules, become important and the simplistic picture needs to be revised. Here, the related case of CO on an amorphous ice surface is considered. The interaction between CO and amorphous ice is important in astronomical contexts where CO-sticking coefficients are of particular interest.[37] Using spatial averaging the likely interaction sites and different ways of binding to the ice surface (dangling and free O–H bonds) are characterized.

The following MC scheme was used with $T=100$ K and for 1000 iterations:

- 500 moves of rigid translation with a maximum distance $x_t^{\max}=0.2$ Å and
- 500 single atom moves applied to C and O atoms of CO with $x_t^{\max}=0.02$ Å.

Initially, simulations were carried out whereby CO was either described with electrostatic and VdW interactions, or only with VdW parameters. This showed that with "electrostatics+VDW" the CO molecule remains largely trapped locally whereas in the second case (VdW only) the molecule was free to move. Therefore the CO motion parallel to the surface is restricted mainly by electrostatic interactions which are dominated by the large quadrupole moment of CO. The displacements of CO on the surface are slightly larger if the water molecules are also allowed to move, which is not further pursued in the following production simulations since no important rearrangements of water molecules take place at the simulation temperature (100 K) and the sampling of favorable positions will not be affected by using a rigid ice surface.

Spatial averaging is applied to the rigid translation at each iteration. The simulation system with sampled CO center of mass (COM) densities on the surface is shown in Fig. 1. It is found that the ice surface is structured and contains several cavities and ridges separating them. Using conventional MC sampling the probe molecule only explores one particular cavity (dark spherical density) whereas spatial averaging with different parameters leads to considerably enhanced exploration of the surface (green and yellow densities, respectively). Corresponding "diffusion curves" according to Eq. (2) are shown in Fig. 2. While for conven-

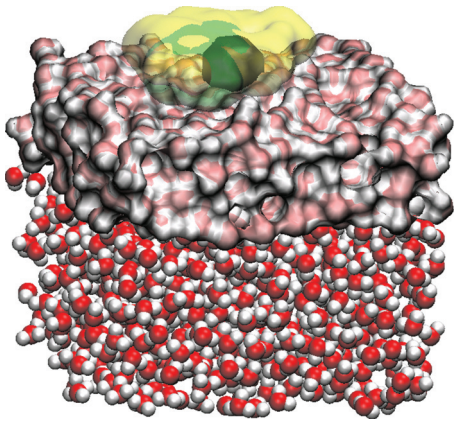

FIG. 1. Ice surface with CO sampling density distribution. The black sphere in the center of the surface shows the distribution for conventional MC sampling, the green density shows the sampling for [2.0,30,30], and the yellow density shows the sampling for [3.0,30,30]. The ice surface is shown in volume representation, layers more distant to the surface are shown in VdW representation.

tional sampling the diffusion is limited (black curves), it increases with increasing width W_ε of the distribution. Changing the number of points N_ε and M_ε also leads to variations in the sampling and sufficiently large values for N_ε and M_ε have to be used. Convergence tests with a smaller number of iterations and a larger number of sampling points showed that results are converged for $[W_\varepsilon,30,30]$.

Detailed analysis shows that conformational space is more efficiently explored by using spatial averaging. Since the free energy surface is modified by the choice of the ε-parameters, it is important to determine whether regions of high sampling densities correspond to energetically favorable positions of the CO on the ice surface. This is analyzed using [3.0,30,30] as an example. The sampled COM positions are projected onto the surface as a two-dimensional map. Then, the surface is divided into squares of 0.5×0.5 Å^2 and the density of sampling points is evaluated for each square. The results are shown in Fig. 3. For the interpretation of such a map it is important to note that the potential used for sampling is a spatially averaged potential. For [3.0,30,30] the average extends over 3 Å. Therefore "structures" corresponding to the points sampled do not necessarily correspond to real low energy configurations, but rather to an average over several favorable positions. Meaningful low energy structures can be found by optimizing representative structures. The position with the highest density is surrounded by three dangling O–H groups. Three structures optimized from initial positions in this region are shown in Fig. 3. For all high density sites, favorable contacts with dangling and bound O–H groups can be found if the structures are optimized based on the initial sampling positions. Such structural properties of favorable sites are in good agreement with favorable positions found from MD simulations in earlier studies.[6]

B. H_2 positions in amorphous ice

Amorphous water ice at low temperatures can incorporate substantial amounts of H_2 which is important for understanding the chemistry and physics of interstellar grain mantles.[38] In addition, the microporous structure of amorphous ice was found to be important for the formation of H_2 (Ref. 8) and the interaction of H_2 molecules with the ice was important to explain H_2 desorption rates.[39] In this context, the migration of H_2 from the bulk to the ice surface is an important step. For hexagonal ice, the diffusion coefficient of H_2 through ice was found to be remarkably high (10^{-5} cm^2/s), comparable to H_2 in liquid and gaseous H_2.[40]

For H_2 in amorphous ice, the following iterative MC scheme was used:

- five moves of rigid translation with different $x_t^{\max}$ and
- ten single atom moves applied to the H-atoms of H_2 with $x_t^{\max}=0.02$ Å.

Results are reported for simulations at 100 K over 10^5 iterations. For the translational part, different maximum translational distances $x_{\max}^t$ were used and the diffusion efficiency was evaluated and compared (see Fig. 4). This is important since the pathways between different favorable positions may involve high energy barriers which cannot easily be surmounted at low temperatures and in a rigid ice matrix. Therefore, the H_2 molecule may remain in the initial cavity for many MC steps. By increasing $x_{\max}^t$, H_2 is able to directly access the next cavity, no matter what the barrier height is. However, the acceptance probability for such a move is low and results in poor sampling. The acceptance ratios correlate well with MC diffusion $\sigma(s)$. For maximal move distances of $x_t^{\max}=4$ Å (Fig. 4, center) the three sets with slow diffusion have acceptance ratios below 1%, whereas the two sets with significantly higher diffusion have acceptance ratios of 22% (magenta) and 35% (orange), respectively.

The system with sampled positions and pathways is shown in Fig. 5. For spatial averaging, the choice of $x_{\max}^t$ is less critical since the barriers can be overcome already for small $x_{\max}^t$ due to averaging of the rapidly changing (rough) potential energy surface. For conventional MC, $x_{\max}^t$ has to be chosen such that the H_2 molecule is able to jump between

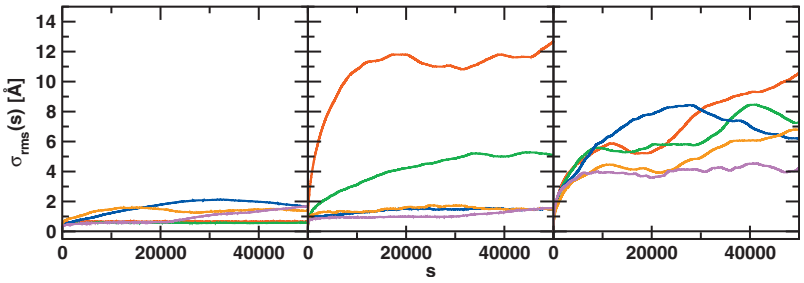

FIG. 2. CO positions on ice surface during 1000 sampling iterations. Comparison of different ε-averaging parameters. $W_\varepsilon=0.5$ Å (left), $W_\varepsilon=1.0$ Å (center), and $W_\varepsilon=2.0$ Å (right). The graphs show the MC diffusion $\sigma(s)$ according to Eq. (2). Conventional MC (black); $[W_\varepsilon,5,6]$ (red); $[W_\varepsilon,10,10]$ (green); $[W_\varepsilon,30,10]$ (blue); $[W_\varepsilon,10,30]$ (orange); $[W_\varepsilon,30,30]$ (magenta).

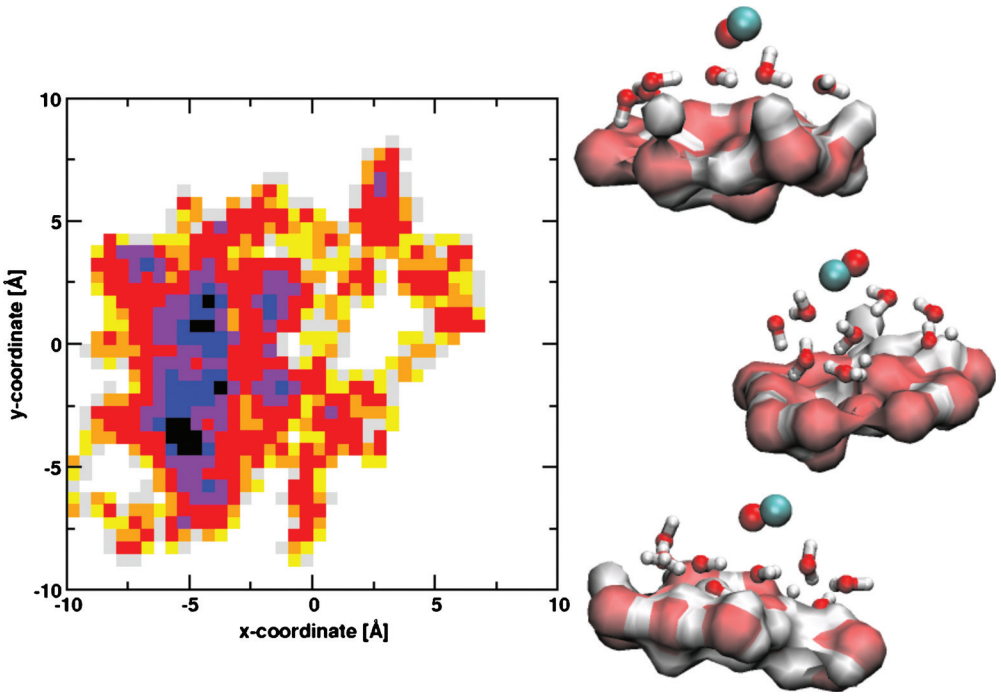

FIG. 3. Density map of CO sampling on ice surface analyzed for $\varepsilon=[3.0,30,30]$. Color coding: 0%–0.01% (gray); 0.01%–0.025% (yellow); 0%–0.025%–0.05% (orange); 0.05%–0.1% (red); 0.1%–0.25% (violet); 0.25%–0.5% (blue); >0.5% (black). Percentages are given with respect to the total (integrated) density. From initial structures in the largest high density region $(-4,-3)$, three optimized structures starting from sampled positions are shown on the right hand side.

different cavities and the sampling therefore depends on $x^t_{\max}$. As a consequence, the comparison of efficiency between conventional MC and spatial averaging also depends on the choice of $x^t_{\max}$. Here, $1 \leq x^t_{\max} \leq 7$ Å is used for different spatial averaging parameters and $\sigma_{\rm rms}$ according to Eq. (2) is individually reported for different $x^t_{\max}$. The results are shown in Fig. 4.

For conventional MC, evaluations of the positions in the ice show that with $x^t_{\max} \leq 3$ Å (not all results shown), the CO remains in the initial cavity. With $x^t_{\max}=4$ Å two cavities are sampled. Increasing $x^t_{\max}$ further leads to H_2 visiting the entire amorphous ice block. For spatial averaging with $W_\varepsilon \geq 1$ Å and $N_\varepsilon > 20$ in contrast, the H_2 leaves the initial cavity for all values of $x^t_{\max}$, starting at $x^t_{\max}=1$ Å. Therefore, the efficiency gain compared to conventional MC is largest for $x^t_{\max}=1$.

For the diffusion of H_2 through amorphous ice, it is of primary interest to characterize the distribution of favorable positions within the ice. For this purpose, the probability distributions $P(\alpha)$ with $\alpha=(x,y,z)$ sampled along the x-, y-,

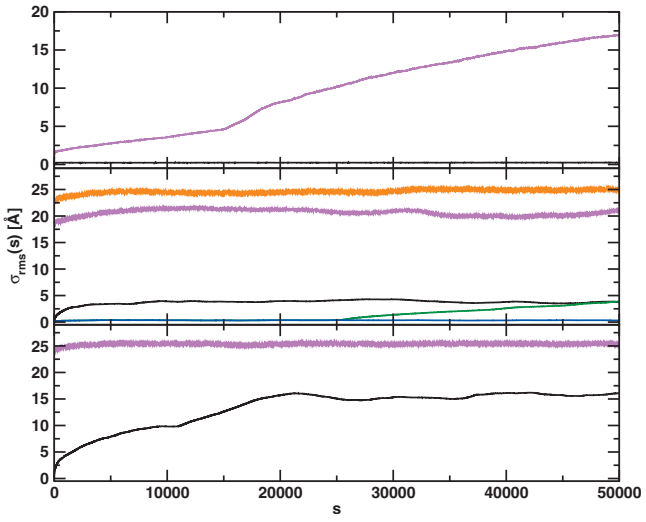

FIG. 4. MC diffusion $\sigma_{\rm rms}(s)$ according to Eq. (2) for H_2 in amorphous ice. Comparison for $W_\varepsilon=2.0$ Å. The MC simulations use different maximum translation distances: $x^t_{\max}=1$ Å (top); $x^t_{\max}=4$ Å (center); $x^t_{\max}=6$ Å (bottom). Conventional MC (black); [2.0,10,10] (green); [2.0,30,10] (blue); [2.0,10,30] (orange); [2.0,30,30] (magenta). Simulations for [2.0,10,10] and [2.0,30,10] (green and blue lines) were only carried out for $x^t_{\max}=4$ Å and are therefore only shown in the center panel.

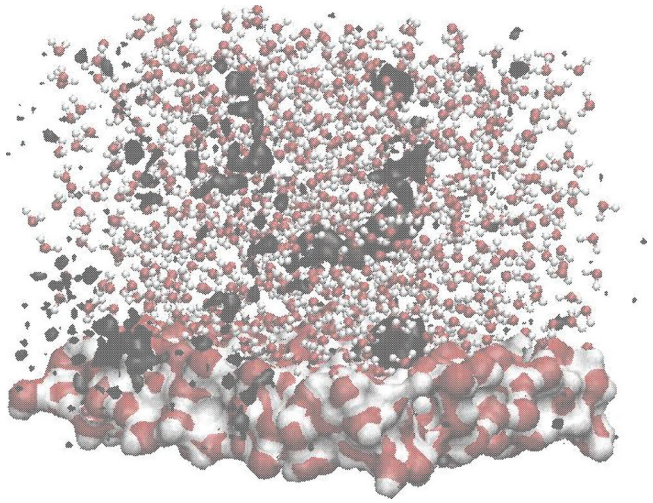

FIG. 5. Sampled positions and pathways for H_2 in amorphous ice. The sampled densities shown in black correspond to 1000 equally distributed H_2 positions taken from the sampling with $x^t_{\max}=6$ Å [2.0,30,30].

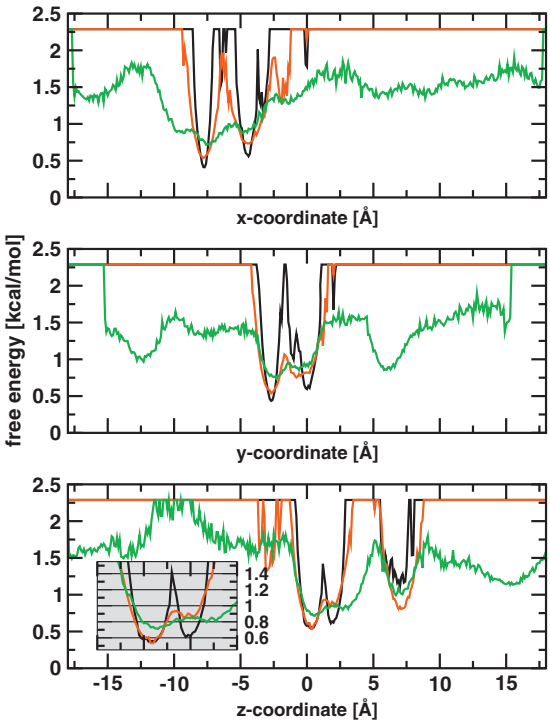

FIG. 6. Free energy profiles for H_2 diffusion in amorphous ice. The profiles are calculated based on the sampling distribution along each of the three axes of the ice cube using x^t_{max}=4 Å. Color coding: Conventional MC (black); [1.0,40,40] (red); [1.5,40,40] (green). The inlay in the bottom panel shows the free energy barrier between minima at z=0.4 and z=2.0 for the different sampling parameters.

and z–coordinates are evaluated and the corresponding free energy profiles are estimated from $G(\alpha)=G_0-k_BT\log P(\alpha)$ (see Fig. 6). Since not all points are sampled, positions with zero occurrence ($P(\alpha)=0$) correspond to high but arbitrary values of $G(\alpha)$. The free energy profiles show a few minima separated by considerable barriers for conventional MC. For spatial averaging, the barriers between the minima are reduced and the free energy profile becomes smoother as W_ε increases. More importantly, additional minima are found which correspond to sampling new cavities. It is interesting to note that the location of the primary minima ($-5\leq x\leq 0$), ($-2.5\leq y\leq 0$), and ($0\leq z\leq 7.5$) characterized with conventional MC, [1.0,40,40] and [1.5,40,40], agree quite well. However, the barriers between the minima are unrealistic by using conventional MC which does not sufficiently sample all cavities in this region. With spatial averaging on the other hand, sampling is much more exhaustive but the barriers are artificially low and depend on W_ε. The inlay in the bottom panel in Fig. 6 shows the dependence of a specific free energy barrier upon increasing W_ε. It reduces from 1 to 0.25 kcal/mol for W_ε=0 (conventional MC) to W_ε=1.5 Å. For other barriers similar observations are made. As an example for the y-axis, the barrier at ($-2.5\leq y\leq 0$) is ≈2 kcal/mol for conventional MC whereas it is considerably reduced to 0.5 and 0.2 kcal/mol by using spatial averaging with increasing W_ε. Assuming that the barriers from spatial averaging are converged, linear extrapolation gives an unbiased barrier of 1.1 kcal/mol. As a result we find that most barriers are below 1 kcal/mol which suggests that the H_2 is diffusing fairly easily in such an environment.

The computed free energy profiles (at T=100 K) can also be compared with results from experiments. In hexagonal ice, quasielastic neutron scattering studies allowed to determine activation energies for H_2 intersite transitions of ≈0.2 kcal/mol.[40] This agrees favorably with the small barriers found for H_2 in amorphous ice (see Fig. 6) and suggests that—once formed—H_2 can indeed diffuse through the solid matrix and be released from the bulk. This is of particular interest to astrophysics because it has been shown that below 70 K UV radiation leads to amorphization of ice.[7]

C. CO in myoglobin

For the two systems discussed above the motion of the surrounding matrix can be treated as fluctuations around an average position because the processes of interest occur at low temperature. This is not true for myoglobin at 300 K, which undergoes conformational changes that can open new diffusion pathways for the CO ligand. For realistic simulations it is thus important to include protein flexibility. Here, this is done by starting MC simulations from an ensemble of different structures obtained from equilibrium MD simulations. A flexible protein matrix can influence ligand diffusion in different ways: Certain positions can become more/less favorable for the CO molecule and therefore decrease/increase the number of transitions to neighboring sites. Also, conformational flexibility can lead to new favorable positions. For the sampling used here, this is not highly probable since to obtain a complete sampling of the conformational space of myoglobin, long MD simulations (or a much larger number of MC moves) are required.[12,13] However, to compare conventional MC with spatial averaging exhaustive sampling is not a prerequisite.

As a starting point for the MC sampling, 100 MD snapshots were generated at 300 K. The simulations were initiated from the equilibrated structure described in Sec. II A, but without the CO ligand present. MD snapshots were then taken every 2 ps. For the MC sampling, the CO ligand was inserted in the distal heme pocket of the first MD snapshot. Next, 1000 MC iterations with five rigid translation and ten single atom moves were applied to the CO molecule. Finally, the CO coordinates were stored and used as initial position to insert the CO in the next MD structure. After insertion in the new MD structure, the entire structure was optimized before performing the next 1000 MC iterations. This procedure was repeated for all MD structures. Different MC parameters were used: x^t_{max}=4, 7, and 10 Å for rigid translation and x^t_{max}=0.02 Å for the single atom moves.

The structure of Mb with the sampled pockets is shown in Fig. 7. Favorable positions in the distal heme pocket and the Xe1 to Xe4 pockets agree well with pockets found from experiment[41] and simulations.[12,13,42] Also, the present MC/MD simulations with spatial averaging (5×10^5 MC moves in total, distributed over 100 protein structures) are able to locate the phantom pockets Ph1 and Ph2 which up to now have only been found by extensive (90 ns) MD simulations.[42] However, the relative population of these

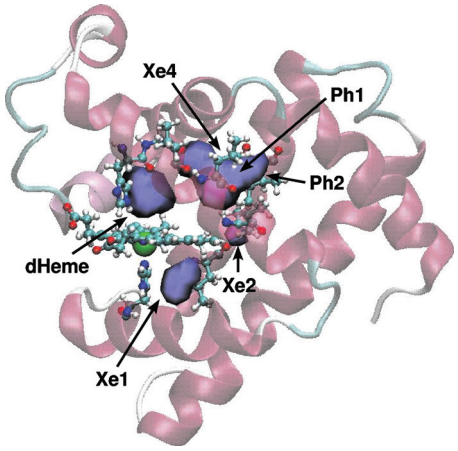

FIG. 7. Myoglobin structure showing the sampled pockets. The COM positions are evaluated over different sampling setups and shown in blue. dHeme refers to the distal heme pocket which is the initial position for the sampling.

states—and hence the free energy difference between them—cannot be expected to be converged due to the limited sampling.

The positions characterized for each sampling strategy are analyzed using a two-dimensional map based on the COM distances between the CO ligand and the C_α of His64 and His93, respectively (see Fig. 8). With conventional MC and for x^t_{max}=4 Å, only the Xe4 and Ph1 pockets are reached. Increasing the maximal translational distance to x^t_{max}=7 Å, the Xe4 and Ph1/Ph2 pockets are found in addition, and for x^t_{max}=10 Å, the CO reaches the Xe1 pocket. Thus, conventional MC samples sites (Xe1, Xe4, and Ph). For spatial averaging with [1.0,20,80], the Xe4 pocket is already reached using x^t_{max}=4. With x^t_{max}=7, the Xe1 and Xe2 pockets are reached in addition and for x^t_{max}=10, the CO escapes to the solvent after sampling several pockets, thus spatial averaging with [1.0,20,80] samples sites (Xe1, Xe2, Xe3, Xe4, Ph, and solvent). Another set of three runs with spatial averaging was carried out with [2.0,20,80] which found sites (Xe1, Xe3, Xe4, Ph, and solvent) and with [1.0,40,40] the same sites could be characterized. Thus, spatial averaging appears also to be fairly robust in view of the particular choice of the parameters used.

The sampling performance for different spatial averaging parameters is further analyzed by considering the MC diffusion σ (see Fig. 9). For x^t_{max}=4 Å, spatial averaging shows a more rapid diffusion and the sampled space is larger. For x^t_{max}=7 Å, the MC diffusion is similar to conventional MC. However, if the positions are analyzed (see above), it is found that spatial averaging samples more different pockets than conventional MC. For x^t_{max}=10 Å, the performance of spatial averaging is also clearly better than for conventional MC. This is seen by the fact that in addition to the favorable positions in the protein, positions in the solvent are sampled.

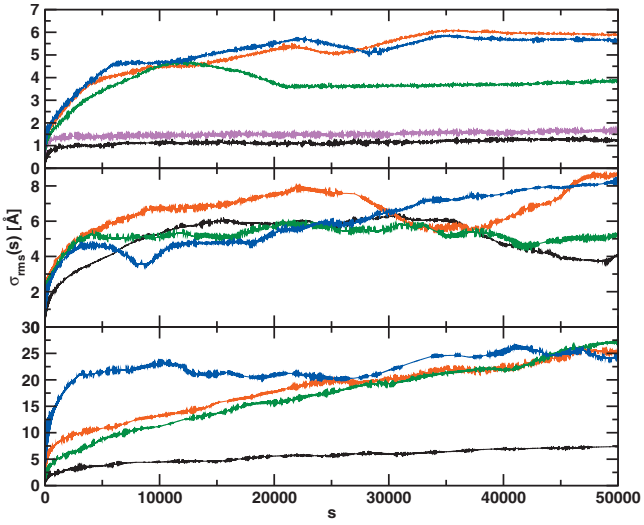

FIG. 9. MC diffusion $\sigma_{rms}(s)$ for MbCO according to Eq. (2) for different spatial averaging parameters. x^t_{max}=4 Å (top), x^t_{max}=7 Å (center), and x^t_{max}=10 Å (bottom). Conventional MC (black); [1.0,30,30] (magenta); [1.0,20,80] (red); [1.0,40,40] (green); [2.0,20,80] (blue).

IV. CONCLUSIONS

A concrete implementation of spatial averaging and its application to sampling small molecules in different heterogeneous and disordered environments is presented. The particular advantage of spatial averaging over other accelerated sampling techniques is that the degrees of freedom that are more efficiently sampled can be directly controlled, but no specific reaction coordinate or other collective variable needs to be defined. For example, in multicanonical sampling[4] the control quantity is the total energy of the system and in umbrella sampling the underlying potential energy function is modified by adding an umbrella potential which involves a "progression variable." In spatial averaging, Eq. (3.4) of Ref. 5 ensures that the thermodynamics of the modified and the original system are closely related. As was shown in Ref. 5, this property is a valuable one in that it tends to avoid the large variance increases that can accompany general "change of measure" methods. With regard to efficiency comparisons it is found that spatial averaging explores the available phase space more efficiently than conventional MC. However, a

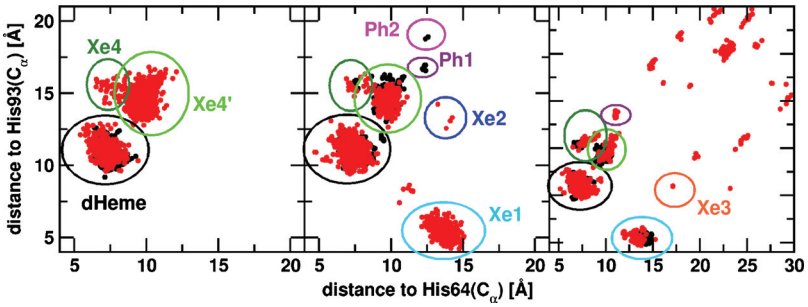

FIG. 8. Distribution of sampling points evaluated as a two-dimensional map, using the distance of the COM to His64 and His93 as coordinates. x^t_{max}=4 Å (left), x^t_{max}=7 Å (middle), and x^t_{max}=10 Å (right). Black corresponds to conventional MC, red corresponds to [1.0,20,80]. The pockets are shown by circles. All positions not enclosed by circles correspond to positions in the solvent. Note the change in scale for panel c.

more detailed comparison-including potential improvement in the implementation-will have to take into account the number of energy evaluations and floating point operations that are required to sample a particular region in space. One possible strategy might be to pre-evaluate the energy difference for a move which would allow to avoiding moves which are very unlikely to be accepted.

The comparison of systems (I)–(III) shows that a significant improvement of the sampling efficiency can be achieved by using spatial averaging for realistic sampling problems. The computational cost of the improvement in terms of number of points used for the averaging depends on the system. For low energy barriers [system (I)] meaningful sampling can already be obtained with a few points (small M_ε and N_ε). With increasing height and steepness of the energy barriers, more sampling points are required. This means that the optimal parameters M_ε and N_ε for spatial averaging somewhat depends on the system. Optimal values for W_ε are remarkably similar for all system and $W_\varepsilon = 2$ Å appears to be a useful choice in all cases studied here.

For CO on amorphous ice, spatial averaging provides efficient sampling of the ice surface. Favorable positions on the surface identified here are in good agreement with positions obtained by unbiased sampling.[6] The barriers for H_2 migration from unbiased sampling (where available) and from spatial averaging simulations are low (≤ 1 kcal/mol) and agree with each other, and are in quite good agreement with previous estimates from experiment.[40] A wider exploration of the available phase space with spatial averaging and subsequent unbiasing of the barriers leads to the same conclusion. However, a full evaluation of the free energy landscape would require more exhaustive sampling. The previously known favorable sites for CO in myoglobin were easily identified using spatial averaging. This is in contrast to conventional MC which was only able to characterize a subset of sites. Also, the regions sampled depended surprisingly little on the translational distance used for the simulations.

Spatial averaging as applied to the systems studied here appears to be a promising method to improve the sampling of complex free energy surfaces arising in a wide range of interesting physical chemical systems. The optimal parameters of W_ε and N_ε depend somewhat on the system under consideration, but are easy to find by a systematic comparison of different parameter sets. For the systems studied here, spatial averaging applied to the moving degrees of freedom considerably improves the sampling efficiency and the degree of improvement depends on the particular system studied.

ACKNOWLEDGMENTS

This work was supported by the Swiss National Science Foundation under Grant No. 200021-117810 (to M.M.) and by the Department of Energy through its Multiscale Mathematics and Optimization for Complex Systems program (award DE-SC0002413, J.D.D. co-PI) and through its Brown University Department of Chemistry award DE-00015561.

[1] A. Laio and M. Parrinello, Proc. Natl. Acad. Sci. U.S.A. **99**, 12562 (2002).
[2] G. M. Torrie and J. P. Valleau, J. Comput. Phys. **23**, 187 (1977).
[3] C. Dellago, P. G. Bolhuis, F. S. Csajka, and D. Chandler, J. Chem. Phys. **108**, 1964 (1998).
[4] B. A. Berg and T. Neuhaus, Phys. Rev. Lett. **68**, 9 (1992).
[5] J. D. Doll, J. E. Gubernatis, N. Plattner, M. Meuwly, P. Dupuis, and H. Wang, J. Chem. Phys. **131**, 104107 (2009).
[6] A. Al-Halabi, H. J. Fraser, G. J. Kroes, and E. F. van Dishoeck, Astron. Astrophys. **422**, 777 (2004).
[7] A. Kouchi and T. Kuroda, Nature (London) **344**, 134 (1990).
[8] E. Mayer and R. Pletzer, Nature (London) **319**, 298 (1986).
[9] R. Elber and M. Karplus, J. Am. Chem. Soc. **112**, 9161 (1990).
[10] J. S. Olson and G. N. Phillips, Jr., J. Biol. Chem. **271**, 17593 (1996).
[11] E. E. Scott, Q. H. Gibson, and J. S. Olson, J. Biol. Chem. **276**, 5177 (2001).
[12] J. Cohen, A. Arkhipov, R. Braun, and K. Schulten, Biophys. J. **91**, 1844 (2006).
[13] J. Z. Ruscio, D. Kumar, M. Shukla, M. G. Prisant, T. M. Murali, and A. V. Onufriev, Proc. Natl. Acad. Sci. U.S.A. **105**, 9204 (2008).
[14] S. Mishra and M. Meuwly, Biophys. J. **96**, 2105 (2009).
[15] O. Carrillo and M. Orozco, Proteins **70**, 892 (2008).
[16] B. R. Brooks, R. E. Bruccoleri, B. D. Olafson, D. J. States, S. Swaminathan, and M. Karplus, J. Comput. Chem. **4**, 187 (1983).
[17] S. Nosé and M. L. Klein, Mol. Phys. **50**, 1055 (1983).
[18] W. G. Hoover, Phys. Rev. A **31**, 1695 (1985).
[19] H. J. C. Berendsen, J. P. M. Postma, W. F. VanGunsteren, A. DiNola, and J. R. Haak, J. Chem. Phys. **81**, 3684 (1984).
[20] J. Kuriyan, S. Wilz, M. Karplus, and G. A. Petsko, J. Mol. Biol. **192**, 133 (1986).
[21] W. L. Jorgensen, J. D. Chandrasekhar, J. D. Madura, R. W. Impey, and M. L. Klein, J. Chem. Phys. **79**, 926 (1983).
[22] W. van Gunsteren and H. Berendsen, Mol. Phys. **34**, 1311 (1977).
[23] M. J. Frisch, G. W. Trucks, H. B. Schlegel, G. E. Scuseria, M. A. Robb, J. R. Cheeseman, J. A. Montgomery, Jr., T. Vreven, K. N. Kudin, J. C. Burant, J. M. Millam, S.E. S. Iyengar, J. Tomasi, V. Barone, B. Mennucci, M. Cossi, G. Scalmani, N. Rega, G. A. Petersson, H. Nakatsuji, M. Hada, M. Ehara, K. Toyota, R. Fukuda, J. Hasegawa, M. Ishida, T. Nakajima, Y. Honda, O. Kitao, H. Nakai, M. Klene, X. Li, J. E. Knox, H. P. Hratchian, J. B. Cross, C. Adamo, J. Jaramillo, R. Gomperts, R. E. Stratmann, O. Yazyev, A. J. Austin, R. Cammi, C. Pomelli, J. W. Ochterski, P. Y. Ayala, K. Morokuma, G. A. Voth, P. Salvador, J. J. Dannenberg, V. G. Zakrzewski, S. Dapprich, A. D. Daniels, M. C. Strain, O. Farkas, D. K. Malick, A. D. Rabuck, K. Raghavachari, J. B. Fo resman, J. V. Ortiz, Q. Cui, A. G. Baboul, S. Clifford, J. Cioslowski, B. B. Stefanov, G. Liu, A. Liashenko, P. Piskorz, I. Komaromi, R. L. Martin, D. J. Fox, T. Keith, M. A. Al Laham, C. Y. Peng, A. Nanayakkara, M. Challacombe, P. M. W. Gill, B. Johnson, W. Chen, M. W. Wong, C. Gonzalez, and J. A. Pople (2004).
[24] A. J. Stone, J. Chem. Theory Comput. **1**, 1128 (2005).
[25] N. Plattner and M. Meuwly, Biophys. J. **94**, 2505 (2008).
[26] A. J. Stone, *The Theory of Intermolecular Forces* (Clarendon, Oxford, 1996).
[27] K. Kuczera, J. Kuriyan, and M. Karplus, J. Mol. Biol. **213**, 351 (1990).
[28] A. D. MacKerell, Jr., D. Bashford, M. Bellott, R. L. Dunbrack, Jr., J. D. Evanseck, M. J. Field, S. Fischer, J. Gao, H. Guo, S. Ha, D. Joseph-McCarthy, L. Kuchnir, K. Kuczera, F. T. K. Lau, C. Mattos, S. Michnick, T. Ngo, D. T. Nguyen, B. Prodhom, W. E. Reiher III, B. Roux, M. Schlenkrich, J. C. Smith, R. Stote, J. E. Straub, M. Watanabe, J. Wiorkiewicz-Kuczera, D. Yin, and M. Karplus, J. Phys. Chem. B **102**, 3586 (1998).
[29] D. J. Earl and M. W. Deem, Phys. Chem. Chem. Phys. **7**, 3910 (2005).
[30] A. R. Dinner, "Monte Carlo simulations of protein folding," Ph.D. thesis, Harvard University, Cambridge, 1999.
[31] D. M. Ceperley and M. Dewing, J. Chem. Phys. **110**, 9812 (1999).
[32] N. Metropolis, A. W. Rosenbluth, M. N. Rosenbluth, A. H. Teller, and E. Teller, J. Chem. Phys. **21**, 1087 (1953).
[33] G. E. P. Box and M. E. Muller, Ann. Math. Stat. **29**, 610 (1958).
[34] N. Plattner and M. Meuwly, ChemPhysChem **9**, 1271 (2008).
[35] P. A. Gerakines, W. A. Schutte, J. M. Greenberg, and E. F. van Dishoeck, Astron. Astrophys. **296**, 810 (1995).
[36] J. Bouwman, W. Ludwig, Z. Awad, K. I. Oeberg, G. W. Fuchs, E. F. van Dishoeck, and H. Linnartz, Astron. Astrophys. **476**, 995 (2007).
[37] S. E. Bisschop, H. J. Fraser, K. I. Oberg, E. F. van Dishoeck, and S. Schlemmer, Astron. Astrophys. **449**, 1297 (2006).
[38] R. W. Dissly, M. Allen, and V. G. Anicich, Astrophys. J. **435**, 685

(1994).
[39] J. E. Roser, S. Swords, G. Vidali, G. Manico, and V. Pirronello, Astrophys. J. **596**, L55 (2003).
[40] H. L. Strauss and Z. Chen, J. Chem. Phys. **101**, 7177 (1994).
[41] R. F. Tilton, I. D. Kuntz, and G. A. Petsko, Biochemistry **23**, 2849 (1984).
[42] C. Bossa, M. Anselmi, D. Roccatano, A. Amadei, B. Vallone, M. Brunori, and A. Di Nola, Biophys. J. **86**, 3855 (2004).